Bioorganic Chemistry 83 (2019) 226–234

Contents lists available at ScienceDirect

Bioorganic Chemistry

journal homepage: www.elsevier.com/locate/bioorg

Synthesis and 2D-QSAR study of dispiropyrrolodinyl-oxindole based alkaloids as cholinesterase inhibitors

Aladdin M. Srour[a,*], Dina H. Dawood[b], Mohammed N.A. Khalil[c], Zienab M. Nofal[a]

[a] Department of Therapeutic Chemistry, Pharmaceutical and Drug Industries Research Division, National Research Centre, Dokki, Giza 12622, Egypt
[b] Chemistry of Natural and Microbial Products Department, Pharmaceutical and Drug Industries Research Division, National Research Centre, Dokki, Giza 12622, Egypt
[c] Pharmacognosy Department, Faculty of Pharmacy, Cairo University, Kasr el Aini St., 11562 Cairo, Egypt

ARTICLE INFO

Keywords:
Oxindole
Acetylcholinesterase
Butyrylcholinesterase
Alzheimer's disease
Donepezil

ABSTRACT

In this work, we describe the regioselective synthesis of some new dispiro[*indene*-2,3′-*pyrrolidine*-2′,3″-*indoline*]-1,2″(3H)-dione **4**-**29** attributable to the previously described methods. All the new chemical entities were assessed *in-vitro* as inhibitors of acetylcholinesterase (AChE) and butyrylcholinesterase (BChE) enzymes; while no significant inhibitory activity for the tested compounds were assigned on AChE, compounds **4**, **27**, **29**, **28** and **15** were the most active against BChE enzyme with IC_{50} = 13.7 μM, 21.8 μM, 22.1 μM, 22.9 μM and 24.9 μM respectively compared to Donepezil (IC_{50} = 0.72 μM). Compound **4** was found to have a mixed type mode of inhibition, the bioactivity of the new chemical entities (N = 26, n = 5, R^2 = 0.893, R^2 cvOO = 0.831, R^2 cvMO = 0.838, F = 33.32, s^2 = 0.003) was elucidated via a statistically significant QSAR model utilizing CODESSA-Pro software that validated the observed results.

1. Introduction

Alzheimer's disease (AD), the most prevalent reason of dementia within the elderly individuals, is a neurodegenerative disturbance distinguished by impairment in cognition, deterioration of memory and disability to carry out the simple routine tasks in life [1]. According to world Alzheimer's reports, more than 46 million individuals worldwide were influenced by this disease in 2015, amid expectations to attain 115 million by 2050 [2]. In spite of all the enormous efforts assigned to the research in this disease, its etiology is still ambiguous. There are various pathophysiological features that are correlated with AD including the accumulation of the neurofibrillary tangles emerged from phosphorylation of tau proteins, extracellular amyloid plaques (Aβ) [3–5] and acetylcholine (ACh) deficiency due to the damage of cholinergic neurons in basal forebrain which lead to the cognitive decline and the lack of short term memory noticed in AD patients [3,4]. Moreover, the oxidative stress was observed as the primary event prior to the incidence of other pathophysiological features of AD [6,7]. The most valuable strategy in curing the symptoms of AD was established on "cholinergic hypothesis" by enhancement Ach level via blocking the cholinesterase enzymes which are involved in hydrolysis of Ach [8,9]. Acetylcholinesterase (AChE) and butyrylcholinesterase (BChE) are two distinct types of cholinesterase enzyme. Both have a similar structure possessing narrow and deep channel which is constituted of five binding zones, (a) peripheral anionic site (PAS) existing at the gorge entry [10] (b) acyl binding site [11] (c) choline binding pocket [12] (d) oxyanion hole [12] and (e) catalytic triad located at the bottom of gorge, where the hydrolysis of acetyl choline occurs [13]. However, there are some variances between them; particularly the size of acyl pocket and this clarifies the reason for substrate diversity between these enzymes. The acyl pocket of AChE is specified by two aromatic amino acids Phe288 and Phe290 which are replaced by small aliphatic amino acids Leu286 and Val288 in BChE [14]. This makes the hollow in the acyl pocket of BChE larger to accommodate the bulky substrates [15]. Despite of minor role of BChE in hydrolysis of ACh in healthy brains, several studies revealed that in the case of AD, BChE activity remarkably increases, while that of AChE decreases [16]. Consequently, both enzymes play a prominent role in the regulation of ACh and they are considered as essential curative targets to increase cholinergic levels [17,18]. The currently available drugs targeting cholinesterase were categorized into selective AChE inhibitors like Donepezil, Galantamine and nonselective inhibitor such as Rivastigmine [19,20]. These drugs ameliorate the cognitive function and the behavior of AD patients. However, the efficacy of these drugs is seriously hampered by various drawbacks such as short duration of action, low bioavailability and high toxicity [21]. Therefore, the discovery of new cholinesterase inhibitors with more efficacy and reduced toxicity is still an imperious demand. It is worth mentioning that the new drugs that serve as dual binding

* Corresponding author.
E-mail address: aladdinsrour@gmail.com (A.M. Srour).

https://doi.org/10.1016/j.bioorg.2018.10.030
Received 19 July 2018; Received in revised form 10 October 2018; Accepted 15 October 2018
Available online 22 October 2018

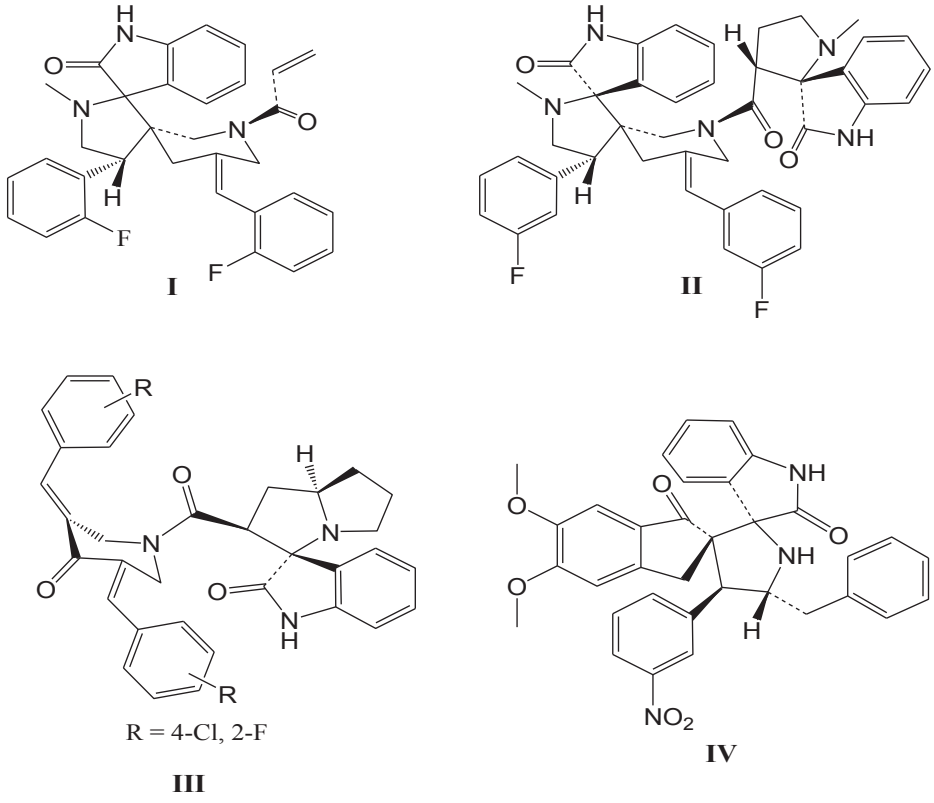

Fig. 1. Structures of spiropyrrolidinyl-oxindole based compounds reported as AChE and BChE inhibitors.

inhibitors for both catalytic active site and PAS of AChE were more efficient in treating AD [22] as they can alleviate cognitive deficits by restoring cholinergic activity and also prevent the deposition of Aβ in the brain promoted by PAS of AChE [23]. Recently, remarkable attention was directed to spiropyrrolidinyl-oxindole based compounds owing to their varied pharmacological properties [24–27] and also attributed to their occurrence as core in many alkaloids with substantial pharmacological efficiency [28–31]. Various studies have demonstrated the effectiveness of spiropyrrolidinyl-oxindole framework in the design of new AChE and BChE inhibitors (Fig. 1) [21,32–34]. Moreover, docking studies of preceding researches disclosed that the hydrophobic interactions of spiropyrrolidinyl-oxindole with amino acid residues in PAS resulting in blocking the entrance of the gorge and forbidding the entry of any substrate into the active site of the enzyme [21,32–34]. Accordingly, spiropyrrolidinyl-oxindole was considered as a vital scaffold among the diverse classes of the newly synthesized cholinesterase inhibitors owing to their dual binding inhibitors efficiency. Incited by the afore-mentioned findings, we interested to synthesize a new set of dispiropyrrolidinyl-oxindole derivatives and validated the observed inhibitory properties versus AChE and BChE enzymes *via* quantitative structure activity relationship (QSAR) studies to determine the most important parameters controlling these properties.

2. Results and discussion

2.1. Chemistry

The synthetic approach for the preparation of new derivatives of dispiroindole scaffolds **4**-**29** is illustrated in Scheme 1, and it is attributable to the previously described methods [24,35,36]. In refluxing ethanol the azomethine ylides **B** formed in situ as a result of decarboxylative condensation of isatines **1a-c** with sarcosin **2**, is further reacted with (α,β-unsaturated) ketones **3a-i** via the classical 1,3-dipolar cycloaddition reaction and in a regioselective manner affording **4**-**29**. The nucleophilic attack of the sarcosin's amino group on the 3-carbonyl function of isatine derivative **1** commences the reaction, followed by dehydration affording the corresponding spirooxazalidinone **A**. Carbon dioxide evicts under the reaction conditions forming a reactive, non-stabilized azomethine ylide **B**, that in situ through 1,3-dipolar cycloaddition to (*E*)-2-arylidene-2,3-dihydro-1*H*-inden-1-one **3**. Then the reaction proceeds in a completely regioselective manner and affords dispiroindole derivatives **4**-**29** as the solitary reaction products (TLC analysis). Structures of the new chemical entities **4**-**29** were assigned as (2S,2′S,4′S)-1″-alkyl-1′-methyl-4′-aryldispiro[*indene*-2,3′-*pyrrolidine*-2′,3″-*indoline*]-1,2″(3H)-dione according to their spectroscopic (IR, ^{1}H, ^{13}C NMR, MS) and elemental analysis data. For instance, a representative of the synthesized dispiroindole series, compound **4** shows intense absorption band at ν = 1689 cm^{-1} referring to the two overlapped carbonyls of ketonic and amidic groups, the ^{1}H NMR spectrum of **4** reveals the ethyl group as triplet and quartet signals at δ_H = 1.12 and δ_H = 3.55 ppm, respectively, and the presence of the diastereotopic protons (two doublets at δ_H = 2.70 and 2.99 ppm) corresponding to the indanyl methylene protons H_2C-3, in addition to appearance of the pyrrolidinyl methylene protons H_2C-5′ as two triplets at δ_H = 3.63 and 4.14 ppm, moreover, the pyrrolidinyl methine proton reveals as a triplet at δ_H = 4.40 ppm. ^{13}C NMR spectrum of **4** shows the ethyl carbons at δ_C = 12.8 and 34.2 attributed to H_3C, H_2C, respectively, the indanyl H_2C-3 at δ_C = 35.2, in addition to two signals at δ_C = 49.9 and 59.1 assigned to the pyrrolidinyl carbons H_2C-4′, H_2C-5′, respectively, furthermore, the spirocarbons *C-2 (C-3′), C-2′ (C-3″)* are detected at δ_C = 66.8 and 77.8, respectively, while the carbonyl carbons of oxindolyl *C-2″* and indanyl *C-1* are resonated at δ_C = 175.9 and 206.5, respectively.

2.2. Anti-cholinesterase activity

The inhibitory activity of the new chemical entities was determined on AChE and BChE at a concentration level of 300 μg/ml (the highest attainable concentration in the assay condition; higher concentrations

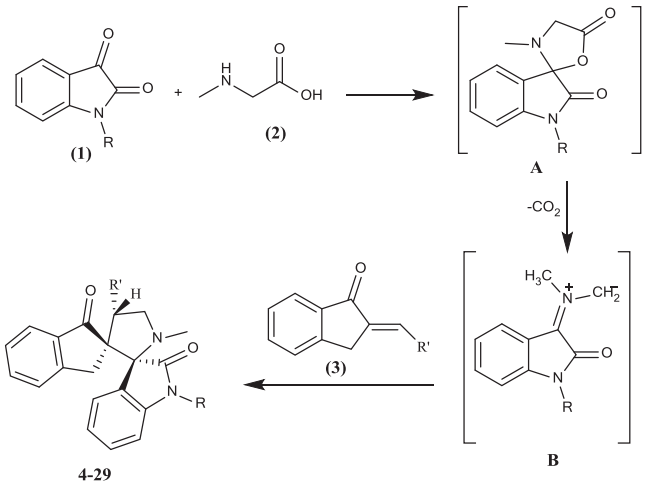

1a; R = C_2H_5
1b; R = C_3H_5
1c; R = C_4H_9

3a; R = Ph
3b; R = 4-ClC_6H_4
3c; R = 4-BrC_6H_4
3d; R = 4-FC_6H_4
3e; R = 4-$H_3CC_6H_4$
3f; R = 4-$H_3COC_6H_4$
3g; R = 3,4,5-$(H_3CO)_3C_6H_2$
3h; R = 4-$N(CH_3)_2C_6H_4$
3i; R = 2-Thienyl

4; R = C_2H_5, R' = C_6H_5
5; R = C_3H_5, R' = C_6H_5
6; R = C_4H_9, R' = C_6H_5
7; R = C_2H_5, R1= 4-ClC_6H_4
8; R = C_3H_5, R' = 4-ClC_6H_4
9; R = C_4H_9, R'= 4-ClC_6H_4
10; R = C_2H_5, R'= 4-BrC_6H_4
11; R = C_3H_5, R'= 4-BrC_6H_4
12; R = C_4H_9, R'= 4-BrC_6H_4
13; R = C_2H_5, R'= 4-FC_6H_4
14; R = C_3H_5, R'= 4-FC_6H_4
15; R = C_4H_9, R'= 4-FC_6H_4
16; R = C_2H_5, R' = 4-$H_3CC_6H_4$
17; R = C_3H_5, R'= 4-$H_3CC_6H_4$
18; R = C_4H_9, R'= 4-$H_3CC_6H_4$
19; R = C_2H_5, R'= 4-$H_3COC_6H_4$
20; R = C_3H_5, R' = 4-$H_3COC_6H_4$
21; R = C_2H_5, R' = 3,4,5-$(H_3CO)_3C_6H_2$
22; R = C_3H_5, R' = 3,4,5-$(H_3CO)_3C_6H_2$
23; R = C_4H_9, R' = 3,4,5-$(H_3CO)_3C_6H_2$
24; R = C_2H_5, R' = 4-$N(CH_3)_2C_6H_4$
25; R = C_3H_5, R' = 4-$N(CH_3)_2C_6H_4$
26; R = C_4H_9, R' = 4-$N(CH_3)_2C_6H_4$
27; R = C_2H_5, R' = 2-Thienyl
28; R = C_3H_5, R' = 2-Thienyl
29; R = C_4H_9, R' = 2-Thienyl

Scheme 1. Synthetic routes towards dispiro[indene-2,3′-pyrrolidine-2′,3″-indoline]-1,2″(3*H*)-dione **4-29**.

showed turbidity and precipitation of assay components). Most of the tested compounds showed higher inhibitory activity against BChE than against AChE (Table 1, Fig. 2). The investigated compounds showed preference for inhibition of BChE, the sets of compounds **4-6**, **13-15** and **27-29** had considerable inhibition compared to the other set of derivatives. However, only compounds **4** and **27** had remarkable inhibitory activity, *ca.* 60%, while compounds **15**, **28** and **29** showed an inhibition which approaches 50% inhibition. Interestingly, a SAR rule have attained, insertion of an ethyl function into oxindolyl ring system with unsubstituted aromatic ring (phenyl and/or thienyl) as in compounds **4** and **27** enhances the inhibitory activity rather than substituted aromatic system, this emphasizes a negative correlation between the

Table 1
Screening of the new chemical entities against BChE and AChE at 300 μg/ml.

Compound	BChE Inhibition (% of inhibition ± SE)[a]	AChE Inhibition (% of inhibition ± SE)[a]
4	73.9 ± 3.84	34.82 ± 8.02
5	48.42 ± 2.1	33.27 ± 4.53
6	37.03 ± 2.04	34.80 ± 2.96
7	23.54 ± 7.01	27.17 ± 5.24
8	22.94 ± 1.02	29.23 ± 7.78
9	28.70 ± 8.44	30.38 ± 4.68
10	37.43 ± 6.26	30.61 ± 1.82
11	39.99 ± 5.73	33.56 ± 8.75
12	17.44 ± 6.40	30.71 ± 6.58
13	43.54 ± 5.76	26.88 ± 4.12
14	45.32 ± 10.06	31.73 ± 4.00
15	53.17 ± 9.8	16.98 ± 1.55
16	28.33 ± 0.86	5.92 ± 3.34
17	37.20 ± 13.62	28.16 ± 4.48
18	40.92 ± 6.70	27.04 ± 3.65
19	38.64 ± 8.60	21.68 ± 2.72
20	38.87 ± 2.26	25.63 ± 4.4
21	36.34 ± 6.92	20.11 ± 5.61
22	36.21 ± 8.13	15.32 ± 3.35
23	28.31 ± 4.43	32.14 ± 6.69
24	36.07 ± 5.07	25.42 ± 2.32
25	37.27 ± 8.48	26.79 ± 4.82
26	38.30 ± 6.98	27.47 ± 2.72
27	66.27 ± 7.38	32.09 ± 4.53
28	57.33 ± 4.55	35.29 ± 3.11
29	57.61 ± 4.70	35.25 ± 2.50
Donepezil	95.90 ± 1.35	97.40 ± 2.4

[a] Average of four replicate correspond to 300 μg/ml.

bulkiness of R‘ and the inhibitory activity. The remarkable reactivity of compounds **4, 27, 28, 29** and **15** incited us to determine their IC_{50} (Table 2), (Fig. S1 in Supplementary material). Compound **4** was the most potent inhibitor because it had the lowest IC_{50} value (13.7 μM); however, it was far from Donepezil, the used reference standard (IC_{50}, 0.72 μM), while the rest compounds had close IC_{50} values, *ca.* 22 μM. Further examination of compound **4** revealed that it had a mixed type mode of inhibition (Fig. 3, Table 3).

2.3. 2D-QSAR

Mathematical transformations of the bio-active agent property values were utilized for 2D-QSAR modeling including log(% inhibition of BChE at 300 μg/ml), BMLC (best multi-linear regression) was initiated stepwise to search for the best n-parameter regression equations, based on the highest R^2 (Squared correlation coefficient) and F (Fisher criteria) values. The 2D-QSAR models with up to 5 descriptors were generated. The statistical parameters including the square of the correlation coefficient (R2), the leave-one-out squared cross-validated correlation coefficient (R^2cv), the Fisher criterion (*F*) and the variance (s2) were used to select the best QSAR model (Table 4). The best observed multi-linear QSAR model for log(% inhibition of BChE at 300 μg/ml)) is displayed in Fig. 4. It is seen that the model is statistically significant and the scatter is uniform, about one logarithmic unit. The descriptors controlling the bio-activity (property) by the established multi-linear QSAR model are arranged, based on their level of significance (*t*-criterion). The first descriptor controlling the BMLR-QSAR model based on its *t*-criterion value ($t = 9.660$) is a CPSA Descriptor the difference between atomic charge weighted partial positive and negative surface areas (DPSA-3) can be determined by Eq. (1) [37].

$$DPSA3 = PPSA3 - -PNSA3 \quad (1)$$

where *PPSA3* is total charge weighted partial positively charged molecular surface area, *PNSA3* is total charge weighted partial negatively charged molecular surface area. Min nucleophilic reactivity index for an N atom (MNRIN) is the second important descriptor controlling the

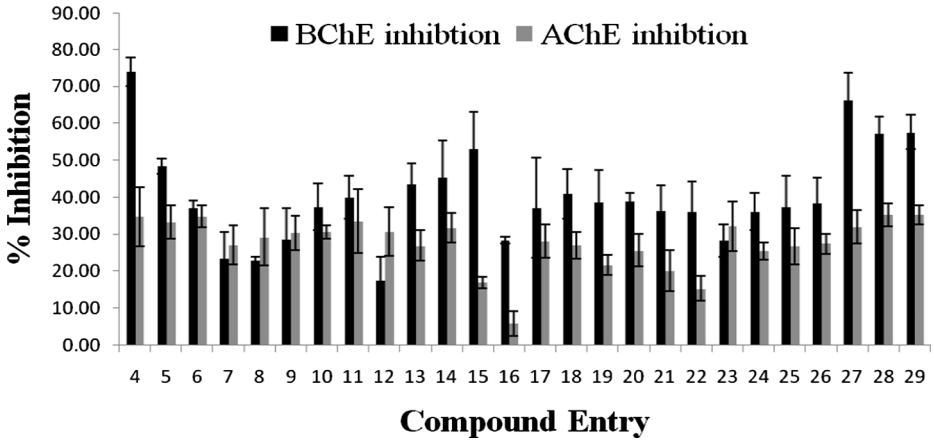

Fig. 2. Inhibitory activity of tested compounds against BChE and AChE.

Table 2
IC_{50} values of BChE inhibitory compounds.

Compound	IC_{50} (μM)[a]
4	13.67 ± 0.5
15	24.9 ± 0.9
27	21.8 ± 0.8
28	22.9 ± 0.9
29	22.1 ± 0.7
Donepezil	0.72 ± 0.1

[a] Average of triplicate.

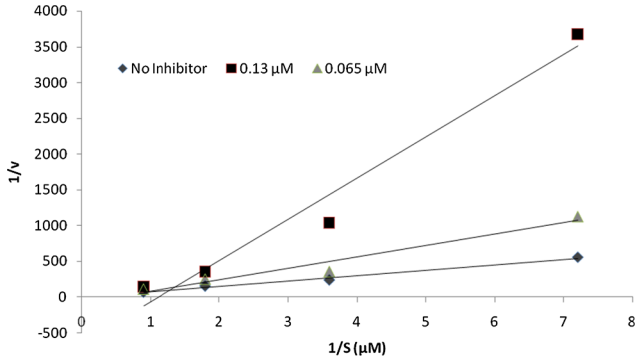

Fig. 3. Lineweaver-Burk plot of BChE inhibtion by compound **4**.

Table 3
Kinetic parameters for BChE inhibition by compound **4**.

Concentration (μM)	K_m (μM)	V_{max} (ΔOD405/min)	K_i
0	17.15	0.225	0.101
0.065	2.01	0.013	
0.13	0.9	0.0016	

BMLR-QSAR model which belongs to charge distribution-related descriptors of quantum chemical descriptors group, it estimates the relative reactivity of the atoms N in the molecule for a given series of compounds and is related to the activation energy of the corresponding chemical reaction [37], Higher the activation energy, harder is the chemical reaction. The positive coefficient in the model (t = 4.086) implies that increasing the value of this descriptor enhances the activity. The third descriptor controlling the 2D-QSAR model based on its t-criterion value (t = 3.236) is Nuclear-electron attraction energy between H and C which is also a quantum chemical descriptor is calculated by Eq. (2) [37].

Table 4
Descriptor of the BMLR-QSAR model for the tested compounds against BChE at 300 μg/ml.

Entry	ID	Coefficient	s	t	Descriptor
1	0	−9.96803	3.627	−2.749	Intercept
2	D1	0.0257319	0.003	9.660	DPSA-3 Difference in CPSAs (PPSA3-PNSA3) (MOPAC PC)
3	D2	34.897	8.541	4.086	Min. nucleoph. react. index for atom N
4	D3	0.172262	0.053	3.236	Min. e-n attraction for bond H−C
5	D4	−0.00687191	0.002	−4.465	HASA-1 (Zefirov PC)
6	D4	−1.17047	0.148	−7.933	Vib. entropy (300 K)/n atoms

N = 26, n = 5, R^2 = 0.893, R^2cvOO = 0.831, R^2cvMO = 0.838, F = 33.32, s^2 = 0.003.
Log(% inhibition of BChE at 300 μg/ml) = −9.96803 + (0.0257319 × D_1) + (34.897 × D_2) + (0.172262 × D_3) − (0.00687191 × D_4) − (1.17047 × D_5).

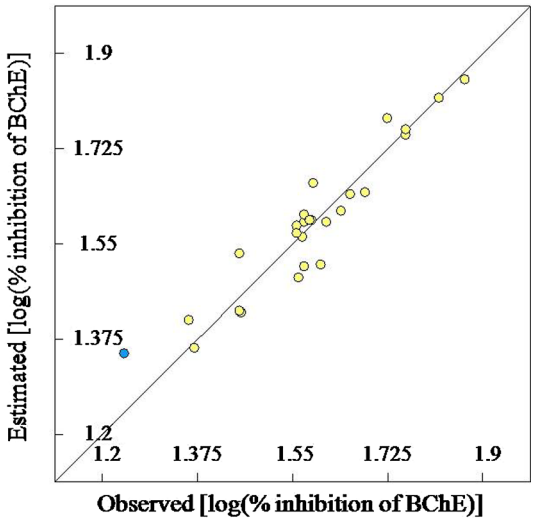

Fig. 4. BMLR-QSAR model plot of correlations representing the observed *vs.* predicted log (% inhibition of BChE) at 300 μg/ml for the tested compounds (Compd. **12** is an outliar).

$$E_{ne}(AB) = \sum_{B} \sum_{\mu,\nu \in A} P_{\mu,\nu} \langle \mu | \frac{Z_B}{R_{iB}} | \rangle \quad (2)$$

where H is given atomic species, C is another atomic species, $P_{\mu,\nu}$ is density matrix elements over atomic basis $\{\mu,\nu\}$, Z_B is charge of atomic nucleus, B, R_{iB} is distance between the electron and atomic nucleus, B and $\langle \mu | \frac{Z_B}{R_{iB}} | \rangle$ is electron-nuclear attraction integrals on atomic basis

{μ,v}. Hydrogen bonding acceptor ability of the molecule HASA-1 (the fourth descriptor controlling the obtained BMLR-QSAR model ($t = -4.465$)), a CPSA descriptor determined by Eq. (3) [37]

$$HASAI = \sum_{A} S_A A \in X_{H-acceptor} \quad (3)$$

where $\frac{S}{D}$ - solvent-accessible surface area of H-bonding acceptor atoms and the fifth important descriptor controlling the BMLR-QSAR model ($t = -7.933$) is a thermodynamical descriptor, vibrational entropy (300 K)/n atoms determined by Eq. (4) [37]

$$S_{vib} = \sum_{j=1}^{\alpha} \{\frac{h\nu_j \exp(-h\nu_j/2kT)}{kT[1-\exp(-h\nu_j/2kT)]} - \ln[1-\exp(-h\nu_j/2kT)]\} \quad (4)$$

Where n_j is frequencies of normal vibrations in the molecule, h is Planck's constant, k is Boltzmann's constant and T is absolute temperature (K). The correlation between the observed and predicted vasodilation activities is represented in Fig. 4. The descriptor values for each respective compound are exhibited in Table S1 of Supplementary material.

The observed correlations due to the internal validation techniques are R^2 cvOO = 0.831, R^2 cvMO = 0.838. Both of them are significantly correlated with the squared correlation coefficient of the attained QSAR model (R^2 = 0.893). Standard deviation of the regressions (s^2 = 0.003) is also a measurable value for the attained model together with the Fisher test value (F = 33.32) that reflects the ratio of the variance explained by the model and the variance due to their errors. A high value of F test compared with the s^2 is a validation of the model. From the results obtained, it is noticeable that, the most potent among all the synthesized analogs compound **4** revealed an observed % of inhibition 73.9% comparable to its experimentally predicted one 71.12% with error 'difference between observed and predicted values' 2.78% while compounds **27**, **28** and **29** as another set of promising analogs shows an observed % of inhibition 66.27%, 57.33% and 57.61%, respectively compared to estimated values 65.81%, 56.15% and 57.30%, respectively with close error values 0.46%, 1.18% and 0.31%, respectively, compound **12** which has the lowest % inhibition among the tested series with an error value = −4.83 for (% inhibition 17.44 and 22.27 for observed and predicted bio-data, respectively), this compound is exhibited as an outlier (Fig. 4), the remaining analogs **5-11**, **13-26** revealed close observed % of inhibition comparable to the estimated ones with error values range −6.87:7.61 which supported the predictive capability of the attained BMLR-QSAR model and validated the previous statement concerning its predictive power due to the statistical values, (Table S1, Fig. S2 in Supplementary material) presented the observed and estimated activity values for the tested compounds against BChE at 300 μg/ml according to the BMLR-QSAR model.

3. Conclusion

In conclusion, *in-vitro* biological assessments of some new dispiropyrrolodinyl-oxindole derivatives **4-29** as inhibitors of acetylcholinesterase (AChE) and butyrylcholinesterase (BChE) enzymes, revealed no significant activity was assigned on AChE, however, on BChE enzyme, compounds **4**, **27**, **29**, **28** and **15** had remarkable activity, with IC_{50} = 13.7 μM, 21.8 μM, 22.1 μM, 22.9 μM and 24.9 μM respectively compared to Donepezil (IC_{50} = 0.72 μM). Then we can conclude that, Insertion of an ethyl function into oxindolyl ring system with unsubstituted aromatic ring (phenyl and/or thienyl) as in the most potent compounds (**4** and **27**) enhances the inhibition activity rather than substituted aromatic system and this emphasizes of a negative correlation between the bulkiness of R and the inhibitory activity, the bioactivity of the new chemical entities (N = 26, n = 5, R^2 = 0.893, R^2 cvOO = 0.831, R^2 cvMO = 0.838, F = 33.32, s^2 = 0.003) was elucidated via a statistically significant QSAR model utilizing CODESSA-Pro software that validated the observed results.

4. Experimental

Melting points were recorded on a Stuart SMP30 melting point apparatus. IR spectra (KBr) were recorded on a JASCO 6100 spectrophotometer. NMR spectra were recorded on a JEOL AS 500 (^{1}H: 500 MHz, ^{13}C: 125 MHz) and a BRUKER 400 (^{1}H: 400, ^{13}C: 100 MHz) spectrometers. Mass spectra were recorded on a Shimadzu GCMS-QP 1000 EX (EI, 70 eV) spectrometer. Compounds **1a-c** [25–27], **3a-i** [25–27] were prepared according to the previously reported procedures (Figs. S3–S104 of Supplementary material put on display the spectral features of the synthesized compounds). Colorimetric enzyme inhibitory assays were performed in 96-well plates and the absorbance was recorded utilizing a microplate reader (Infinite F50, Tecan, Switzerland).

*4.1. Synthesis of dispiro[indene-2,3′-pyrrolidine-2′,3″-indoline]-1,2″(3H)-dione **4-29***

General procedure

Equimolar quantities of 2-(arylmethylidene)-2,3-dihydro-1*H*-inden-1-ones **3a-i** (5 mmol), the appropriate isatin **1a-c** and sarcosine **2** were heated under reflux for the specified time in ethanol (25 mL). The separated solid was collected and crystallized from a suitable solvent affording the corresponding **4-29**.

*4.1.1. (2S,2′S,4′S)-1″-ethyl-1′-methyl-4′-phenyldispiro[indene-2,3′-pyrrolidine-2′,3″-indoline]-1,2″(3H)-dione **(4)***

Colorless microcrystals from ethanol; yield 1.2 g (57%); mp 158–160 °C; IR: ν_{max}/cm^{-1} 1689, 1609, 1457. ^{1}H NMR (400 MHz, $CDCl_3$): δ 1.12 (t, J = 7.2 Hz, 3H), 2.20 (s, 3H), 2.70 (d, J = 17.6 Hz, 1H), 2.99 (d, J = 17.6 Hz, 1H), 3.55 (q, J = 6.9 Hz, 2H), 3.63 (t, J = 8.8, 1H), 4.14 (t, J = 9.4 Hz, 1H), 4.40 (t, J = 9.0 Hz, 1H), 6.56 (d, J = 8 Hz, 1H), 6.92–7.42 (m, 11H), 7.46 (d, J = 8 Hz, 1H). ^{13}C NMR (100 MHz, $CDCl_3$): δ 12.8, 34.2, 35.2, 49.9, 59.1, 66.8, 77.8, 107.6, 122.6, 123.8, 125.3, 125.4, 127.0, 127.1, 127.5, 128.3, 128.4, 129.2, 130.1, 134.5, 135.7, 139.1, 143.0, 151.6, 175.9, 206.5. MS: *m/z* (%) 422 (M, 8), 202 (100). Anal. Calcd. for $C_{28}H_{26}N_2O_2$ (422.52): C, 79.59; H, 6.20; N, 6.63, found C, 79.45; H, 6.27; N, 6.52.

*4.1.2. (2S,2′S,4′S)-1″-allyl-1′-methyl-4′-phenyldispiro[indene-2,3′-pyrrolidine-2′,3″-indoline]-1,2″(3H)-dione **(5)***

Colorless microcrystals from ethanol; yield 1.3 g (60%); mp 133–135 °C; IR: ν_{max}/cm^{-1} 1701, 1608, 1456. ^{1}H NMR (400 MHz, $CDCl_3$): δ 2.21 (s, 3H), 2.70 (d, J = 17.6 Hz, 1H), 2.96 (d, J = 18.0 Hz, 1H), 3.65 (t, J = 8.8 Hz, 1H), 4.09–4.15 (m, 3H), 4.33–4.42 (m, 1H), 5.06, 5.12 (dd, J = 17.2, 10.0 Hz, 2H), 5.65–5.75 (m,1H), 6.53 (d, J = 7.2 Hz, 1H), 6.92–7.43 (m, 11H), 7.48 (d, J = 7.2 Hz, 1H). ^{13}C NMR (100 MHz, $CDCl_3$): δ 22.8, 35.2, 35.3, 41.7, 50.0, 59.2, 66.8, 78.0, 108.4, 117.4, 122.7, 123.9, 125.3, 127.0, 127.2, 127.3, 128.4, 129.1, 130.1, 131.2, 134.5, 135.7, 139.2, 143.2, 151.6, 176.2, 206.7. MS: *m/z* (%) 434 (M, 23), 201 (100) Anal. Calcd. for $C_{29}H_{26}N_2O_2$ (434.53): C, 80.16; H, 6.03; N, 6.45, found C, 80.05; H, 6.14; N, 6.51.

*4.1.3. (2S,2′S,4′S)-1″-butyl-1′-methyl-4′-phenyldispiro[indene-2,3′-pyrrolidine-2′,3″-indoline]-1,2″(3H)-dione **(6)***

Colorless microcrystals from ethanol; yield 1.22 g (54%); mp 127–129 °C; IR: ν_{max}/cm^{-1} 1704, 1610, 1456. ^{1}H NMR (400 MHz, $CDCl_3$): δ 0.93 (t, J = 7.2 Hz, 3H), 1.24–1.36 (m, 2H), 1.46–1.54 (m, 2H), 2.20 (s, 3H), 2.70 (d, J = 17.6 Hz, 1H), 2.99 (d, J = 17.6 Hz, 1H), 3.47–3.70 (m, 3H), 4.15 (t, J = 9.6 Hz, 1H), 4.41 (t, J = 9.0 Hz, 1H), 6.57 (d, J = 7.2 Hz, 1H), 6.93–7.42 (m, 11H), 7.47 (d, J = 7.2 Hz, 1H). ^{13}C NMR (100 MHz, $CDCl_3$): δ 13.8, 20.2, 29.6, 35.2, 39.4, 49.9, 59.0, 66.7, 77.9, 107.8, 122.6, 123.9, 125.2, 127.0, 127.1, 127.5, 128.4, 129.2, 130.1, 134.5, 135.7, 139.1, 143.5, 151.6, 176.0, 206.5. MS: *m/z* (%) 450 (M, 6), 229 (100). Anal. Calcd. for $C_{30}H_{30}N_2O_2$ (450.57): C,

79.97; H, 6.71; N, 6.22, found C, 80.04; H, 6.86; N, 6.10.

*4.1.4. (2S,2′S,4′S)-4′-(4-chlorophenyl)-1″-ethyl-1′-methyldispiro[indene-2,3′-pyrrolidine-2′,3″-indoline]-1,2″(3H)-dione (**7**)*

Colorless microcrystals from ethanol; yield 1.60 g (70%); mp 166–168 °C; IR: ν_{max}/cm^{-1} 1705, 1609, 1457. ^{1}H NMR (500 MHz, $CDCl_3$): δ 1.11 (t, J = 7.2 Hz, 3H), 2.15 (s, 3H), 2.65 (d, J = 17.2 Hz, 1H), 2.91 (d, J = 17.2 Hz, 1H), 3.57 (q, J = 7.3 Hz, 2H), 3.74 (t, J = 7.2 Hz, 1H), 4.04 (t, J = 9.6 Hz, 1H), 4.31 (t, J = 8.6 Hz, 1H), 6.56 (d, J = 7.7 Hz, 1H), 6.91–7.40 (m, 10H), 7.52 (d, J = 7.7 Hz, 1H). ^{13}C NMR (125 MHz, $CDCl_3$): δ 12.9, 34.3, 35.1, 35.3, 49.4, 59.4, 66.7, 77.4, 107.7, 122.7, 124.0, 125.3, 127.3, 127.5, 128.6, 129.3, 131.6, 132.9, 134.4, 135.8, 137.9, 143.2, 151.4, 176.2, 206.5. MS: *m/z* (%) 457 (M + 1, 8), 456 (M, 3), 202 (100). Anal. Calcd. for $C_{28}H_{25}ClN_2O_2$ (456.96): C, 73.59; H, 5.51; N, 6.13, found C, 73.50; H, 5.66; N, 6.17.

*4.1.5. (2S,2′S,4′S)-1″-allyl-4′-(4-chlorophenyl)-1′-methyldispiro[indene-2,3′-pyrrolidine-2′,3″-indoline]-1,2″(3H)-dione (**8**)*

Colorless microcrystals from ethanol; yield 1.60 g (68%); mp 161–163 °C; IR: ν_{max}/cm^{-1} 1705, 1610, 1461. ^{1}H NMR (500 MHz, $CDCl_3$): δ 2.17 (s, 3H), 2.65 (d, J = 17.2 Hz, 1H), 2.910 (d, J = 17.2 Hz, 1H), 3.62 (t, J = 8.6 Hz, 1H), 4.04 (t, J = 9.6 Hz, 1H), 4.12 (d, J = 12.4 Hz, 2H), 4.32 (t, J = 9.1 Hz, 1H), 5.06, 5.13 (dd, J = 17.2, 10.5 Hz, 2H), 5.68–5.73 (m, 1H), 6.54 (d, J = 7.7 Hz, 1H), 6.92–7.39 (m, 10H), 7.48 (d, J = 7.7 Hz, 1H). ^{13}C NMR (125 MHz, $CDCl_3$): δ 35.2, 35.4, 41.8, 49.5, 59.4, 66.6, 77.4, 108.5, 117.5, 122.9, 124.0., 125.4, 127.4, 128.6, 129.3, 131.2, 131.6, 133.2, 134.7, 135.8, 138.0, 143.8, 151.3, 176.3, 206.6. MS: *m/z* (%) 469 (M + 1, 12), 468 (M, 6), 301 (100). Anal. Calcd. for $C_{29}H_{25}ClN_2O_2$ (468.97): C, 74.27; H, 5.37; N, 5.97, found C, 74.12; H, 5.30; N, 6.04.

*4.1.6. (2S,2′S,4′S)-1″-butyl-4′-(4-chlorophenyl)-1′-methyldispiro[indene-2,3′-pyrrolidine-2′,3″-indoline]-1,2″(3H)-dione (**9**)*

Colorless microcrystals from ethanol; yield 1.65 g (68%); mp 155–156 °C; IR: ν_{max}/cm^{-1} 1701, 1616, 1457. ^{1}H NMR (400 MHz, $CDCl_3$): δ 0.96 (t, J = 7.2 Hz, 3H), 1.24–1.37 (m, 2H), 1.48–1.6256 (m, 2H), 2.20 (s, 3H), 2.66 (d, J = 17.6 Hz, 1H), 2.94 (d, J = 18.0 Hz, 1H), 3.48–3.56 (m, 2H), 3.66 (t, J = 7.4 Hz, 1H), 4.10 (t, J = 8.8 Hz, 1H), 4.36 (t, J = 8.8 Hz, 1H), 6.57 (d, J = 8 Hz, 1H), 6.92–7.45 (m, 10H), 7.48 (d, J = 8 Hz, 1H). MS: *m/z* (%) 484 (M − 1, 2), 229 (100). Anal. Calcd. for $C_{30}H_{29}ClN_2O_2$ (485.02): C, 74.29; H, 6.03; N, 5.78, found C, 74.17; H, 6.20; N, 5.60.

*4.1.7. (2S,2′S,4′S)-4′-(4-bromophenyl)-1″-ethyl-1′-methyldispiro[indene-2,3′-pyrrolidine-2′,3″-indoline]-1,2″(3H)-dione (**10**)*

Colorless microcrystals from ethanol; yield 1.81 g (72%); mp 162–163 °C; IR: ν_{max}/cm^{-1} 1704, 1617, 1458. ^{1}H NMR (500 MHz, $CDCl_3$): δ 1.13 (t, J = 7.2 Hz, 3H), 2.17 (s, 3H), 2.64 (d, J = 18.2 Hz, 1H), 2.92 (d, J = 18.2 Hz, 1H), 3.57 (q, J = 6.7 Hz, 2H), 3.75 (t, J = 7.2 Hz, 1H), 4.05 (t, J = 9.4 Hz, 1H), 4.30 (t, J = 8.6 Hz, 1H), 6.57 (d, J = 7.7 Hz, 1H), 6.93–7.39 (m, 10H), 7.47 (d, J = 7.7 Hz, 1H). ^{13}C NMR (125 MHz, $CDCl_3$): δ 12.9, 34.3, 35.1, 35.3, 49.5, 59.3, 66.6, 77.4, 107.7, 121.2, 122.7, 124.0, 125.4, 127.3, 127.5, 129.3, 131.6, 132.0, 134.7, 135.8, 138.2, 143.2, 151.4, 176.1, 206.5. MS: *m/z* (%) 501 (M, 2), 289 (1 0 0). Anal. Calcd. for $C_{28}H_{25}BrN_2O_2$ (501.41): C, 67.07; H, 5.03; N, 5.59, found C, 67.12; H, 5.10; N, 5.50.

*4.1.8. (2S,2′S,4′S)-1″-allyl-4′-(4-bromophenyl)-1′-methyldispiro[indene-2,3′-pyrrolidine-2′,3″-indoline]-1,2″(3H)-dione (**11**)*

Colorless microcrystals from ethanol; yield 1.90 g (74%); mp 156–157 °C; IR: ν_{max}/cm^{-1} 1704, 1608, 1482. ^{1}H NMR (500 MHz, $CDCl_3$): δ 2.17 (s, 3H), 2.64 (d, J = 17.2 Hz, 1H), 2.89 (d, J = 18.2 Hz, 1H), 3.59 (t, J = 8.6 Hz, 1H), 4.04 (t, J = 9.5 Hz, 1H), 4.13 (d, J = 12.4 Hz, 2H), 4.30 (t, J = 9.6 Hz, 1H), 5.03 (dd, J = 17.2, 10.5 Hz, 2H), 5.67–5.73 (m, 1H), 6.55 (d, J = 7.7 Hz, 1H), 6.70–7.38 (m, 10H), 7.42 (d, J = 7.7 Hz, 1H). ^{13}C NMR (125 MHz, $CDCl_3$): δ 35.2, 35.4, 41.8, 49.6, 59.3, 66.6, 77.4, 108.5, 117.5, 120.8, 122.9, 124.0, 125.4, 127.4, 129.3, 131.2, 131.6, 132.0, 134.7, 135.8, 138.4, 143.4, 151.3, 176.3, 206.5. MS: *m/z* (%) 512 (M − 1, 12), 302 (100). Anal. Calcd. for $C_{29}H_{25}BrN_2O_2$ (513.42): C, 67.84; H, 4.91; N, 5.46, found C, 67.70; H, 4.99; N, 5.59.

*4.1.9. (2S,2′S,4′S)-4′-(4-bromophenyl)-1″-butyl-1′-methyldispiro[indene-2,3′-pyrrolidine-2′,3″-indoline]-1,2″(3H)-dione (**12**)*

Colorless microcrystals from ethanol; yield 1.70 g (64%); mp 157–158 °C; IR: ν_{max}/cm^{-1} 1702, 1613, 1458. ^{1}H NMR (500 MHz, $CDCl_3$): δ 0.92 (t, J = 7.2 Hz, 3H), 1.24–1.52 (m, 4H), 2.15 (s, 3H), 2.64 (d, J = 17.2 Hz, 1H), 2.92 (d, J = 18.2 Hz, 1H), 3.51–3.64 (m, 3H), 4.04 (t, J = 9.6 Hz, 1H), 4.30 (t, J = 9.1 Hz, 1H), 6.55 (d, J = 7.6 Hz, 1H), 6.91–7.38 (m, 10H), 7.47 (d, J = 7.6 Hz, 1H). ^{13}C NMR (125 MHz, $CDCl_3$): δ 13.8, 20.3, 29.7, 35.3, 39.5, 49.5, 59.3, 66.5, 77.4, 107.8, 121.0, 122.6, 124.0, 125.4, 127.4, 129.2, 131.6, 132.0, 134.7, 135.8, 138.5, 143.6, 151.4, 176.3, 206.5. MS: *m/z* (%) 529 (M, 38), 318 (100). Anal. Calcd. for $C_{30}H_{29}BrN_2O_2$ (529.47): C, 68.05; H, 5.52; N, 5.29, found C, 68.17; H, 5.63; N, 5.20.

*4.1.10. (2S,2′S,4′S)-1″-ethyl-4′-(4-fluorophenyl)-1′-methyldispiro [indene-2,3′-pyrrolidine-2′,3″-indoline]-1,2″(3H)-dione (**13**)*

Colorless microcrystals from ethanol; yield 1.70 g (77%); mp 138–139 °C; IR: ν_{max}/cm^{-1} 1706, 1607, 1464. ^{1}H NMR (400 MHz, $CDCl_3$): δ 1.14 (t, J = 7.4 Hz, 3H), 2.20 (s, 3H), 2.66 (d, J = 17.6 Hz, 1H), 2.93 (d, J = 17.6 Hz, 1H), 3.56 (q, J = 7.1 Hz, 2H), 3.71–3.80 (m, 1H), 4.08 (t, J = 9.2 Hz, 1H), 4.36 (t, J = 9.0 Hz, 1H), 6.58 (d, J = 8 Hz, 1H), 6.93–7.44 (m, 10H), 7.84 (d, J = 7.2 Hz, 1H). ^{13}C NMR (100 MHz, $CDCl_3$): δ 12.8, 34.2, 35.2, 49.3, 59.3, 66.5, 77.8, 107.7, 115.1, 115.3, 122.7, 123.9, 125.2, 127.2, 127.6, 129.3, 131.6, 131.7, 134.6, 134.8, 135.7, 143.0, 151.4, 160.7, 163.1, 206.5. MS: *m/z* (%) 441 (M + 1, 14), 202 (1 0 0). Anal. Calcd. for $C_{28}H_{25}FN_2O_2$ (440.51): C, 76.34; H, 5.72; N, 6.36, found C, 76.18; H, 5.80; N, 6.50.

*4.1.11. (2S,2′S,4′S)-1″-allyl-4′-(4-fluorophenyl)-1′-methyldispiro[indene-2,3′-pyrrolidine-2′,3″-indoline]-1,2″(3H)-dione (**14**)*

Colorless microcrystals from ethanol; yield 1.57 g (69%); mp 149–150 °C; IR: ν_{max}/cm^{-1} 1707, 1610, 1457. ^{1}H NMR (400 MHz, $CDCl_3$): δ 2.17 (s, 3H), 2.69 (d, J = 18.0 Hz, 1H), 2.93 (d, J = 18.4 Hz, 1H), 3.71 (t, J = 7.2 Hz, 1H), 4.12–4.17 (m, 3H), 4.34, 4.39 (dd, J = 5.2, 4.8 Hz, 1H), 5.08, 5.16 (dd, J = 17.2, 10.0 Hz, 2H), 5.67–5.76 (m, 1H), 6.56 (d, J = 8 Hz, 1H), 6.95–7.41 (m, 10H), 7.50 (d, J = 7.2 Hz, 1H). MS: *m/z* (%) 452 (M, 7), 301 (100). Anal. Calcd. for $C_{29}H_{25}FN_2O_2$ (452.52): C, 76.97; H, 5.57; N, 6.19, found C, 76.80; H, 5.79; N, 6.30.

*4.1.12. (2S,2′S,4′S)-1″-butyl-4′-(4-fluorophenyl)-1′-methyldispiro [indene-2,3′-pyrrolidine-2′,3″-indoline]-1,2″(3H)-dione (**15**)*

Colorless microcrystals from ethanol, yield 1.55 g (66%); mp 135–136 °C; IR: ν_{max}/cm^{-1} 1703, 1617, 1458. ^{1}H NMR (500 MHz, $CDCl_3$): δ 0.92 (t, J = 7.2 Hz, 3H), 1.24–1.52 (m, 4H), 2.16 (s, 3H), 2.64 (d, J = 18.2 Hz, 1H), 2.91 (d, J = 18.2 Hz, 1H), 3.52–3.66 (m, 3H), 4.05 (t, J = 9.1 Hz, 1H), 4.32 (t, J = 9.1 Hz, 1H), 6.56 (d, J = 7.7 Hz, 1H), 6.92–7.39 (m, 10H), 7.48 (d, J = 6.7 Hz, 1H). ^{13}C NMR (125 MHz, $CDCl_3$): δ 13.8, 20.3, 29.7, 35.2, 39.5, 49.4, 59.5, 66.6, 77.4, 107.9, 115.2, 115.3, 122.6, 124.0, 125.3, 127.3, 129.6, 131.7, 134.6, 135.1, 135.8, 143.6, 151.5, 161.0, 162.9, 176.4, 206.7. MS: *m/z* (%) 468 (M, 3), 229 (1 0 0). Anal. Calcd. for $C_{30}H_{29}FN_2O_2$ (468.56): C, 76.90; H, 6.24; N, 5.98, found C, 76.95; H, 6.12; N, 5.90.

*4.1.13. (2S,2′S,4′S)-1″-ethyl-1′-methyl-4′-(p-tolyl)dispiro[indene-2,3′-pyrrolidine-2′,3″-indoline]-1,2″(3H)-dione (**16**)*

Colorless microcrystals from ethanol; yield 1.2 g (55%); mp 134–135 °C; IR: ν_{max}/cm^{-1} 1706, 1606, 1462. ^{1}H NMR (400 MHz, $CDCl_3$): δ 1.10 (t, J = 7.2 Hz, 3H), 2.19 (s, 3H), 2.29 (s, 3H), 2.71 (d, J = 17.6 Hz, 1H), 2.99 (d, J = 17.6 Hz, 1H), 3.50–3.63 (m, 1H), 3.75

(q, J = 7.1 Hz, 2H), 4.11 (t, J = 9.4 Hz, 1H), 4.38 (t, J = 9.0 Hz, 1H), 6.56 (d, J = 7.6 Hz, 1H), 6.92–7.30 (m, 9H), 7.41 (d, J = 6.8 Hz, 1H), 7.46 (d, J = 8 Hz, 1H), ^{13}C NMR (100 MHz, $CDCl_3$): δ 12.8, 21.0, 34.2, 35.1, 35.2, 49.5, 59.1, 66.8, 77.9, 107.6, 122.5, 123.8, 125.3, 127.1, 127.5, 129.1, 129.9, 134.4, 135.8, 136.0, 136.6, 142.9, 151.7, 175.9, 206.6. MS: *m/z* (%) 436 (M, 6), 201 (100). Anal. Calcd. for $C_{29}H_{28}N_2O_2$ (436.54): C, 79.79; H, 6.46; N, 6.42, found C, 79.69; H, 6.40; N, 6.49.

4.1.14. (2S,2′S,4′S)-1″-allyl-1′-methyl-4′-(p-tolyl)dispiro[indene-2,3′-pyrrolidine-2′,3″-indoline]-1,2″(3H)-dione ***(17)***

Colorless microcrystals from ethanol; yield 1.30 g (58%); mp 114–115 °C; IR: ν_{max}/cm^{-1} 1707, 1606, 1464. ^{1}H NMR (500 MHz, $CDCl_3$): δ 2.18 (s, 3H), 2.27 (s, 3H), 2.71 (d, J = 17.2 Hz, 1H), 2.97 (d, J = 18.2 Hz, 1H), 3.59 (t, J = 10.5 Hz, 1H), 4.09–4.11 (m, 3H), 4.36 (t, J = 9.6 Hz, 1H), 5.04, 5.11 (dd, J = 17.2, 9.6 Hz, 2H), 5.66–5.71 (m, 1H), 6.53 (d, J = 7.7 Hz, 1H), 6.93–7.52 (m, 11H). ^{13}C NMR (125 MHz, $CDCl_3$): δ 21.1, 35.3, 35.4, 41.8, 49.8, 59.3, 66.9, 77.4, 108.5, 117.4, 122.8, 124.0, 125.4, 127.2, 127.4, 129.1, 129.2, 130.1, 131.3, 134.6, 135.8, 136.3, 136.8, 143.7, 151.8, 176.3, 206.9. MS: *m/z* (%) 449 (M + 1, 12), 448 (M, 5), 213 (100). Anal. Calcd. for $C_{30}H_{28}N_2O_2$ (448.56): C, 80.33; H, 6.29; N, 6.25, found C, 80.42; H, 6.20; N, 6.33.

4.1.15. (2S,2′S,4′S)-1″-butyl-1′-methyl-4′-(p-tolyl)dispiro[indene-2,3′-pyrrolidine-2′,3″-indoline]-1,2″(3H)-dione ***(18)***

Colorless microcrystals from ethanol, yield 1.25 g (54%); mp 115–117 °C; IR: ν_{max}/cm^{-1} 1712, 1618, 1458. ^{1}H NMR (400 MHz, $CDCl_3$): δ 0.92 (t, J = 7.4 Hz, 3H), 1.24–1.52 (m, 4H), 2.17 (s, 3H), 2.29 (s, 3H), 2.71 (d, J = 17.6 Hz, 1H), 2.99 (d, J = 17.6 Hz, 1H), 3.46–3.70 (m, 3H), 4.10 (t, J = 9.4 Hz, 1H), 4.37 (t, J = 9.2 Hz, 1H), 6.56 (d, J = 8 Hz, 1H), 6.92–7.31 (m, 9H), 7.39 (d, J = 7.2 Hz, 1H), 7.46 (d, J = 7.6 Hz, 1H). ^{13}C NMR (100 MHz, $CDCl_3$): δ 13.8, 20.2, 21.0, 29.6, 35.2, 39.4, 49.6, 59.1, 66.8, 77.9, 107.7, 122.5, 123.8, 124.4, 125.3, 125.5, 126.1, 127.1, 127.6, 129.1, 129.7, 129.9, 130.8, 134.4, 135.8, 136.1, 136.5, 143.5, 151.8, 176.2, 206.7. MS: *m/z* (%) 465 (M + 1, 40), 464 (M, 11), 229 (100). Anal. Calcd. for $C_{31}H_{32}N_2O_2$ (464.60): C, 80.14; H, 6.94; N, 6.03, found C, 80.27; H, 6.87; N, 6.10.

4.1.16. (2S,2′S,4′S)-1″-ethyl-4′-(4-methoxyphenyl)-1′-methyldispiro[indene-2,3′-pyrrolidine-2′,3″-indoline]-1,2″(3H)-dione ***(19)***

Colorless microcrystals from ethanol; yield 1.45 g (64%); mp 139–140 °C; IR: ν_{max}/cm^{-1} 1715, 1688, 1609, 1463. ^{1}H NMR (400 MHz, $CDCl_3$): δ 1.12 (t, J = 7.4 Hz, 3H), 2.19 (s, 3H), 2.72 (d, J = 17.6 Hz, 1H), 2.94 (d, J = 17.6 Hz, 1H), 3.55 (q, J = 6.9 Hz, 2H), 3.72 (t, J = 7.2 Hz, 1H), 3.76 (s, 3H), 4.08 (t, J = 9.4 Hz, 1H), 4.34 (t, J = 9.0 Hz, 1H), 6.57 (d, J = 7.6 Hz, 1H), 6.8 (d, J = 8.8 Hz, 2H), 6.93–7.48 (m, 9H). MS: *m/z* (%) 453 (M + 1, 6), 202 (100). Anal. Calcd. for $C_{29}H_{28}N_2O_3$ (452.54): C, 76.97; H, 6.24; N, 6.19, found C, 76.90; H, 6.37; N, 6.25.

4.1.17. (2S,2′S,4′S)-1″-allyl-4′-(4-methoxyphenyl)-1′-methyldispiro[indene-2,3′-pyrrolidine-2′,3″-indoline]-1,2″(3H)-dione ***(20)***

Colorless microcrystals from ethanol; yield 1.40 g (60%); mp 125–126 °C; IR: ν_{max}/cm^{-1} 1705, 1605, 1458. ^{1}H NMR (500 MHz, $CDCl_3$): δ 2.19 (s, 3H), 2.72 (d, J = 18.2 Hz, 1H), 2.92 (d, J = 17.2 Hz, 1H), 3.61 (t, J = 9.1 Hz, 1H), 3.76 (s, 3H), 4.06 (t, J = 9.6 Hz, 1H), 4.12 (d, J = 16.2 Hz, 2H), 4.33 (t, J = 9.1 Hz, 1H), 5.05, 5.13 (dd, J = 17.2, 10.5 Hz, 2H), 5.68–5.73 (m, 1H), 6.54 (d, J = 7.78 Hz, 1H), 6.79 (d, J = 8.6 Hz, 2H), 6.93–7.41 (m, 8H), 7.49 (d, J = 7.7 Hz, 1H). ^{13}C NMR (125 MHz, $CDCl_3$): δ 35.3, 41.8, 49.6, 55.2, 59.4, 66.9, 77.5, 108.5, 113.8, 117.4, 122.8, 123.9, 125.4, 127.2, 127.5, 129.4, 131.2, 131.3, 134.5, 135.8, 143.3, 151.7, 158.6, 176.3, 206.9. MS: *m/z* (%) 464 (M, 3), 289 (100). Anal. Calcd. for $C_{30}H_{28}N_2O_3$ (464.55): C, 77.56; H, 6.08; N, 6.03, found C, 77.43; H, 6.00; N, 6.10.

4.1.18. (2S,2′S,4′S)-1″-ethyl-1′-methyl-4′-(3,4,5-trimethoxyphenyl)dispiro[indene-2,3′-pyrrolidine-2′,3″-indoline]-1,2″(3H)-dione ***(21)***

Colorless microcrystals from ethanol; yield 1.90 g (74%); mp 145–147 °C; IR: ν_{max}/cm^{-1} 1715, 1697, 1462. ^{1}H NMR (400 MHz, $CDCl_3$): δ 1.12 (t, J = 7.4 Hz, 3H), 2.19 (s, 3H), 2.68 (d, J = 18.0 Hz, 1H), 2.92 (d, J = 17.6 Hz, 1H), 3.56 (q, J = 7.1 Hz, 2H), 3.74 (t, J = 7.2 Hz, 1H), 3.76 (s, 6H), 3.80 (s, 3H), 4.10 (t, J = 9.6 Hz, 1H), 4.27 (t, J = 8.8 Hz, 1H), 6.56 (d, J = 7.2 Hz, 1H), 6.65 (s, 1H), 6.92–7.32 (m, 6H), 7.41 (d, J = 7.2 Hz, 1H), 7.48 (d, J = 7.6 Hz, 1H). ^{13}C NMR (100 MHz, $CDCl_3$): δ 12.8, 34.1, 35.1, 35.2, 50.4, 56.1, 59.0, 60.8, 66.8, 77.7, 106.8, 107.7, 122.5, 123.9, 125.4, 127.1, 127.5, 129.1, 134.5, 134.8, 135.8, 136.7, 143.0, 152.0, 152.9, 175.9, 206.8. MS: *m/z* (%) 512 (M, 5), 202 (100). Anal. Calcd. for $C_{31}H_{32}N_2O_5$ (512.60): C, 72.64; H, 6.29; N, 5.47, found C, 72.90; H, 6.37; N, 5.55.

4.1.19. (2S,2′S,4′S)-1″-allyl-1′-methyl-4′-(3,4,5-trimethoxyphenyl)dispiro[indene-2,3′-pyrrolidine-2′,3″-indoline]-1,2″(3H)-dione ***(22)***

Colorless microcrystals from ethanol; yield 1.84 g (70%); mp 188–189 °C; IR: ν_{max}/cm^{-1} 1706, 1606, 1461. ^{1}H NMR (400 MHz, $CDCl_3$): δ 2.20 (s, 3H), 2.69 (d, J = 18.0 Hz, 1H), 2.90 (d, J = 17.6 Hz, 1H), 3.64 (t, J = 8.6 Hz, 1H), 3.76 (s, 6H), 3.10 (s, 3H), 4.10 (t, J = 9.2 Hz, 1H), 4.15 (d, J = 4.8 Hz, 2H), 4.25–4.36 (m 1H), 5.06, 5.15 (dd, J = 17.2, 10.8 Hz, 2H), 5.67–5.74 (m, 1H), 6.54 (d, J = 7.6 Hz, 1H), 6.63 (s, 1H), 6.92–7.34 (m, 6H), 7.41 (d, J = 7.2 Hz, 1H), 7.50 (d, J = 7.2 Hz, 1H). ^{13}C NMR (100 MHz, $CDCl_3$): δ 35.2, 35.3, 41.7, 50.5, 56.1, 59.0, 60.8, 66.7, 77.8, 106.8, 108.5, 117.4, 122.7, 124.0, 125.0, 125.4, 127.1, 127.4, 129.1, 131.2, 134.6, 134.8, 135.8, 136.7, 143.2, 151.9, 153.0, 176.1, 206.9. MS: *m/z* (%) 524 (M, 2), 310 (100). Anal. Calcd. for $C_{32}H_{32}N_2O_5$ (524.61): C, 73.26; H, 6.15; N, 5.34, found C, 73.42; H, 6.24; N, 5.43.

4.1.20. (2S,2′S,4′S)-1″-butyl-1′-methyl-4′-(3,4,5-trimethoxyphenyl)dispiro[indene-2,3′-pyrrolidine-2′,3″-indoline]-1,2″(3H)-dione ***(23)***

Colorless microcrystals from ethanol, yield 1.73 g (64%); mp 173–174 °C; IR: ν_{max}/cm^{-1} 1709, 1598, 1457. ^{1}H NMR (400 MHz, $CDCl_3$): δ 0.94 (t, J = 7.2 Hz, 3H), 1.22–1.54 (m, 4H), 2.20 (s, 3H), 2.69 (d, J = 18.0 Hz, 1H), 2.93 (d, J = 18.0 Hz, 1H), 3.44–3.75 (m, 2H), 3.77 (s, 6H), 3.80 (s, 3H), 3.94 (t, J = 10.4 Hz, 1H), 4.10 (t, J = 8.2 Hz, 1H), 4.30 (t, J = 8.6 Hz, 1H), 6.57 (d, J = 8 Hz, 1H), 6.67 (s, 1H), 6.92–7.66 (m, 8H). MS: *m/z* (%) 540 (M, 3), 230 (100). Anal. Calcd. for $C_{33}H_{36}N_2O_5$ (540.65): C, 73.31; H, 6.71; N, 5.18, found C, 73.50; H, 6.87; N, 5.10.

4.1.21. (2S,2′S,4′S)-4′-(4-(dimethylamino)phenyl)-1″-ethyl-1′-methyldispiro[indene-2,3′-pyrrolidine-2′,3″-indoline]-1,2″(3H)-dione ***(24)***

Yellow microcrystals from *n*-butanol; yield 1.33 g (57%); mp 192–193 °C; IR: ν_{max}/cm^{-1} 1702, 1609, 1461. ^{1}H NMR (400 MHz, DMSO-d_6): δ 0.90 (t, J = 7.0 Hz, 3H), 1.98 (s, 3H), 2.59 (d, J = 18.0 Hz, 1H), 2.81 (s, 6H), 3.10 (d, J = 18.8 Hz, 1H), 3.64 (q, J = 7.1 Hz, 2H), 3.84 (t, J = 9.2, 1H), 4.16 (t, J = 9.0 Hz, 1H), 4.31 (t, J = 5.2 Hz, 1H), 6.61 (d, J = 8.8 Hz, 1H), 6.78 (d, J = 7.6 Hz, 1H), 6.90 (d, J = 7.4 Hz, 1H), 7.10–7.39 (m, 9H). ^{13}C NMR (100 MHz, DMSO-d_6): δ 12.9, 34.1, 34.6, 35.1, 40.6, 48.9, 58.9, 66.9, 77.6, 108.6, 112.8, 122.3, 123.4, 125.8, 126.2, 126.6, 127.0, 127.7, 129.6, 130.5, 135.2, 135.7, 143.1, 149.8, 151.9, 175.6, 206.2. MS: *m/z* (%) 465 (M, 58), 202 (100). Anal. Calcd. for $C_{30}H_{31}N_3O_2$ (465.59): C, 77.39; H, 6.71; N, 9.03, found C, 77.45; H, 6.93; N, 9.22.

4.1.22. (2S,2′S,4′S)-1″-allyl-4′-(4-(dimethylamino)phenyl)-1′-methyldispiro[indene-2,3′-pyrrolidine-2′,3″-indoline]-1,2″(3H)-dione ***(25)***

Yellow microcrystals from DMF; yield 1.29 g (54%); mp 157–159 °C; IR: ν_{max}/cm^{-1} 1710, 1609, 1457. ^{1}H NMR (400 MHz, DMSO-d_6): δ 1.99 (s, 3H), 2.61 (d, J = 18 Hz, 1H), 2.81 (s, 6H), 3.0 (d, J = 18.0 Hz, 1H), 3.41 (t, J = 8.6 Hz, 1H), 3.84 (t, J = 9.2 Hz, 1H), 4.01–4.18 (m, 1H) 4.30 (d, J = 11.6 Hz, 2H), 4.92, 5.03 (dd, J = 17.2, 10.0 Hz, 2H), 5.62–5.69 (m, 1H), 6.60 (d, J = 8.8 Hz, 1H), 6.67 (d, J = 7.6 Hz, 1H),

6.90 (d, J = 7.6 Hz, 1H), 7.07–7.39 (m, 9H). ^{13}C NMR (100 MHz, DMSO-d_6): δ 34.8, 35.1, 40.6, 41.5, 49.1, 58.9, 66.7, 77.8, 109.3, 112.7, 117.1, 122.5, 123.5,123.7, 125.5, 126.2, 126.5, 127.0, 127.8, 129.5,130.6, 132.2, 133.2, 134.6, 135.3, 135.7, 143.4, 149.8, 151.8, 175.8, 206.4. MS: m/z (%) 476 (M−1, 5), 263 (100). Anal. Calcd. for $C_{31}H_{31}N_3O_2$ (477.60): C, 77.96; H, 6.54; N, 8.80, found C, 77.73; H, 6.70; N, 8.90.

4.1.23. (2S,2′S,4′S)-1″-butyl-4′-(4-(dimethylamino)phenyl)-1′-methyldispiro[indene-2,3′-pyrrolidine-2′,3″-indoline]-1,2″(3H)-dione (26)

Yellow microcrystals from ethanol, yield 1.24 g (50%); mp 163–164 °C; IR: ν_{max}/cm^{-1} 1712, 1618, 1458. ^{1}H NMR (400 MHz, $CDCl_3$): δ 0.92 (t, J = 7.2 Hz, 3H), 1.22–1.48 (m, 4H), 2.17 (s, 3H), 2.79 (d, J = 17.6 Hz, 1H), 2.89 (s, 6H), 2.98 (d, J = 17.6 Hz, 1H), 3.48–3.73 (m, 3H), 4.07 (t, J = 9.2 Hz, 1H), 4.32 (t, J = 8.6 Hz, 1H), 6.56 (d, J = 7.6 Hz, 1H), 6.65 (d, J = 8.4 Hz, 1H), 6.71–7.63 (m, 10H). ^{13}C NMR (100 MHz, $CDCl_3$): δ 13.8, 20.2, 29.6, 35.2, 39.4, 40.6, 49.5, 59.1, 66.9, 77.9, 107.7, 112.6, 122.4, 123.7, 125.3, 125.7, 127.0, 127.5, 129.0, 130.7, 130.9, 134.3, 135.9, 143.5, 149.5, 152.0, 176.2, 207.0. MS: m/z (%) 493 (M, 8), 263 (100). Anal. Calcd. for $C_{32}H_{35}N_3O_2$ (493.64): C, 77.86; H, 7.15; N, 8.51, found C, 77.69; H, 7.28; N, 8.40.

4.1.24. (2S,2′S,4′S)-1″-ethyl-1′-methyl-4′-(thiophen-2-yl)dispiro[indene-2,3′-pyrrolidine-2′,3″-indoline]-1,2″(3H)-dione (27)

Colorless microcrystals from ethanol; yield 1.35 g (63%); mp 144–146 °C; IR: ν_{max}/cm^{-1} 1691, 1617, 1461. ^{1}H NMR (400 MHz, $CDCl_3$): δ 1.11 (t, J = 7.2 Hz, 3H), 2.20 (s, 3H), 2.83 (d, J = 18.0 Hz, 1H), 2.96 (d, J = 18.0 Hz, 1H), 3.57 (q, J = 7.1 Hz, 2H), 3.69–3.77 (m, 1H), 4.13 (t, J = 9.4 Hz, 1H), 4.63 (t, J = 9.0 Hz, 1H), 6.61 (d, J = 7.6 Hz, 1H), 6.90–7.44 (m, 9H), 7.53 (d, J = 7.6 Hz, 1H). ^{13}C NMR (100 MHz, $CDCl_3$): δ 12.8, 34.2, 34.5, 35.2, 45.0, 59.8, 66.2, 77.6, 107.8, 122.6, 124.0, 124.8, 125.4, 126.5, 126.9, 127.1, 127.2, 127.6, 129.3, 134.7, 135.7, 142.4, 143.1, 152.2, 175.6, 206.3. MS: m/z (%) 428 (M, 13), 290 (100). Anal. Calcd. for $C_{26}H_{24}N_2O_2S$ (428.55): C, 72.87; H, 5.64; N, 6.54; S, 7.48, found C, 73.00; H, 5.70; N, 6.64; S, 7.54.

4.1.25. (2S,2′S,4′S)-1″-allyl-1′-methyl-4′-(thiophen-2-yl)dispiro[indene-2,3′-pyrrolidine-2′,3″-indoline]-1,2″(3H)-dione (28)

Colorless microcrystals from ethanol; yield 1.5 g (68%); mp 130–132 °C; IR: ν_{max}/cm^{-1} 1701, 1602, 1456. ^{1}H NMR (400 MHz, $CDCl_3$): δ 2.20 (s, 3H), 2.84 (d, J = 18.4 Hz, 1H), 2.97 (d, J = 18.0 Hz, 1H), 3.75 (t, J = 8.8 Hz, 1H), 4.12 (t, J = 9.2 Hz, 1H), 4.32, 4.36 (dd, J = 5.6, 6.4 Hz, 2H), 4.63 (t, J = 8.8 Hz, 1H), 5.05, 5.10 (dd, J = 17.2, 10.4 Hz, 2H), 5.65–5.74 (m, 1H), 6.50 (d, J = 8 Hz, 1H), 6.590–7.45 (m, 9H), 7.50 (d, J = 8 Hz, 1H). ^{13}C NMR (100 MHz, $CDCl_3$): δ 32.3, 34.7, 35.2, 41.7, 45.0, 59.9, 66.1, 77.7, 108.6, 117.5, 122.8, 124.1, 124.8, 125.4, 126.9, 127.1, 127.2, 127.5, 127.7, 129.3, 131.2, 134.7, 135.7, 142.4, 143.4, 152.1, 175.8, 206.3. MS: m/z (%) 440 (M, 6), 214 (100). Anal. Calcd. for $C_{27}H_{24}N_2O_2S$ (440.56): C, 73.61; H, 5.49; N, 6.36; S,7.28, found C, 73.54; H, 5.58; N, 6.40; S, 7.35.

4.1.26. (2S,2′S,4′S)-1″-butyl-1′-methyl-4′-(thiophen-2-yl)dispiro[indene-2,3′-pyrrolidine-2′,3″-indoline]-1,2″(3H)-dione (29)

Colorless microcrystals from ethanol; yield 1.30 g (57%); mp 157–158 °C; IR: ν_{max}/cm^{-1} 1690, 1617, 1462. ^{1}H NMR (400 MHz, $CDCl_3$): δ 0.92 (t, J = 7.4 Hz, 3H), 1.24–1.53 (m, 4H), 2.17 (s, 3H), 2.83 (d, J = 18.0 Hz, 1H), 2.96 (d, J = 18.0 Hz, 1H), 3.49–3.94 (m, 3H), 4.13 (t, J = 9.6 Hz, 1H), 4.64 (t, J = 9.0 Hz, 1H), 6.60 (d, J = 8 Hz, 1H), 6.90–7.63 (m, 9H), 7.89 (t, J = 3 Hz, 1H). ^{13}C NMR (100 MHz, $CDCl_3$): δ 13.8, 20.2, 29.7, 35.2, 39.4, 45.0, 59.8, 66.1, 77.6, 107.9, 122.5, 124.0, 124.3, 124.7, 125.4, 126.9, 127.1, 127.2, 127.7, 129.2, 130.5, 134.7, 135.8, 142.5, 143.6, 149.0, 193.8. MS: m/z (%) 456 (M, 4), 230 (100). Anal. Calcd. for $C_{28}H_{28}N_2O_2S$ (456.60): C, 73.65; H, 6.18; N, 6.14, S; 7.02, found C, 73.50; H, 6.26; N, 6.20, S; 7.07.

4.2. Estimation of the inhibitory activity against acetylcholine esterase (AChE) and butyrylcholine esterase (BChE) enzymes

The assays were conducted using 96-well plate, as reported previously with little modifications [32], the enzyme inhibition assays were performed in Tris-HCl buffer (200 mM, pH 7.5). First, the buffer (170 µl) was added followed by the tested compound (20 µl, in MeOH solution). The enzyme solution (20 µl) was added; it was prepared at concentration level (0.1 U/ml) in the same buffer but containing 0.1% bovine serum albumin. After 10 min incubation at 25 °C, the indicator (40 µl) was added, dithio-bis-(2-nitrobenzoic acid) DTNB (0.69 mM in tris buffer). The reaction started by addition of the specified substrate (1.11 mM) at volume of 20 µl. Butyrylthiocholine iodide was utilized in BChE assays, while acetylthiocholine was utilized in AChE assays. The reaction was left for 10 min and the intensity of the developed color was measured at 405 nm (reading A). Control assays without the inhibitor were performed by replacing the tested compound by MeOH (20 µl) and their absorbance values were recorded (Reading B). Blank assays contained the same composition but the enzyme (20 µl) was replaced by buffer, their absorbances were used to correct for spontaneous lysis of the indicator or inherent color of the inhibitor. Absorbences were recorded using a microplate reader.

$$\% \text{ of inhibition} = (1 - (\text{corrected A}/\text{corrected B})) * 100.$$

4.3. Enzyme kinetics and mode of inhibition

Lineweaver-Burk plot analysis was utilized to determine the mode of inhibition of compound 4 against BChE enzyme. Plots were constructed at inhibitor concentration levels (0.0, 0.065 and 0.13 µM) over concentrations of substrate (1.11, 0.56, 0.27, 0.14 µM). Ki was calculated using GraphPad Prism software utilizing the equation adopted for mixed type of inhibition [38].

$$\text{VmaxApp} = \text{Vmax}/(1 + \text{I}/(\text{Alpha} * \text{Ki}))$$
$$\text{KmApp} = \text{Km} * (1 + \text{I}/\text{Ki})/(1 + \text{I}/(\text{Alpha} * \text{Ki}))$$

$Y = \text{VmaxApp} * X/(\text{KmApp} + X)$ The parameter I is the concentration of inhibitor. The parameters Alpha, Vmax, Km and Ki were determined by Prism which fits one best-fit value for the entire set of data.

Appendix A. Supplementary material

Supplementary data to this article can be found online at https://doi.org/10.1016/j.bioorg.2018.10.030.

References

[1] H. Tang, H.-T. Zhao, S.-M. Zhong, Z.-Y. Wang, Z.-F. Chen, H. Liang, Novel oxoisoaporphine-based inhibitors of acetyl- and butyrylcholinesterase and acetylcholinesterase-induced beta-amyloid aggregation, Bioorg. Med. Chem. Lett. 2 (2012) 2257–2261.
[2] https://www.alz.co.uk/research/worldalzheimerreport2016sheet (09.01.2018).
[3] A.C. Nordberg, Biological markers and the cholinergic hypothesis in Alzheimer's disease, Acta Neurol. Scand. 139 (1992) 54–58.
[4] A.V. Terry, J.J. Buccafusco, the cholinergic hypothesis of age and Alzheimer's disease-related cognitive deficits: recent challenges and their implications for novel drug development, J. Pharmacol. Exp. Ther. 306 (2003) 821–827.
[5] J.D.L. Torre, Is Alzheimer's disease a neurodegenerative or a vascular disorder Data, dogma, and dialectics, Lancet Neurol. 3 (2004) 184–190.
[6] S. Varadarajan, S. Yatin, M. Aksenova, D.A. Butterfield, Review: Alzheimer's amyloid beta–peptide-associated free radical oxidative stress and neurotoxicity, J. Struct. Biol. 130 (2000) 184–208.
[7] X. Wang, W. Wang, L. Li, G. Perry, H. Lee, X. Zhu, Oxidative stress and mitochondrial dysfunction in Alzheimer's disease, Biochim. Biophys. Acta 2014 (1842) 1240–1247.
[8] J.L. Cummings, Alzheimer's disease, N. Engl. J. Med. 351 (2004) 56–67.
[9] N. Tabet, Acetylcholinesterase inhibitors for Alzheimer's disease: anti-inflammatories in acetylcholine clothing, Age Ageing 35 (2006) 336–338.
[10] P. Axelsen, M. Harel, I. Silman, J. Sussman, Structure and dynamics of the active site gorge of acetylcholinesterase: synergistic use of molecular dynamics simulation

and X-ray crystallography, Protein Sci. 3 (1994) 188–197.
[11] M. Harel, D.M. Quinn, H.K. Nair, I. Silman, J.L. Sussman, The X-ray structure of a transition state analog complex reveals the molecular origins of the catalytic power and substrate specificity of acetylcholinesterase, JACS 118 (1996) 2340–2346.
[12] J.L. Sussman, M. Harel, F. Frolow, C. Oefner, A. Goldman, L. Toker, I. Silman, Atomic structure of acetylcholinesterase from Torpedo californica: a prototypic acetylcholine-binding protein, Science 253 (1991) 872–879.
[13] B.A. Yankner, New clues to Alzheimer's disease: Unraveling the roles of amyloid and tau, Nat. Med. 2 (1996) 850–852.
[14] A.N. Cokugras, Butyrylcholinesterase: structure and physiological importance, Turk. J. Biochem. 28 (2003) 54–61.
[15] Y. Nicolet, O. Lockridge, P. Masson, J.C. Fontecilla-Camps, F. Nachon, Crystal structure of human butyryl cholinesterase and of its complexes with substrate and products, J. Biol. Chem. 278 (2003) 41141–41147.
[16] A. Ciro, J. Park, G. Burkhard, N. Yan, C. Geula, Biochemical differentiation of cholinesterases from normal and Alzheimer's disease cortex, Curr. Alzheimer Res. 9 (2012) 138–143.
[17] R. León, A.G. García, J. Marco-Contelles, Recent advances in the multi targetdirected ligands approach for the treatment of Alzheimer's disease, Med. Res. Rev. 33 (2013) 139–189.
[18] D. Dolles, M. Nimczick, M. Scheiner, J. Ramler, P. Stadtmuller, E. Sawatzky, A. Drakopoulos, C. Sotriffer, H.J. Wittmann, A. Strasser, M. Decker, Aminobenzimidazoles and structural isomers as templates for dual-acting butyrylcholinesterase inhibitors and hCB2 R ligands to combat neurodegenerative disorders, Chem. Med. Chem. 11 (2016) 1270–1283.
[19] B.M. McGleenon, K.B. Dynan, A.P. Passmore, Acetylcholinesterase inhibitors in Alzheimer's disease, Br. J. Clin. Pharmacol. 48 (1999) 471–480.
[20] S.G. Di Santo, F. Prinelli, F. Adorni, C. Caltagirone, M. Musicco, A meta-analysis of the efficacy of donepezil, rivastigmine, galantamine, and memantine in relation to severity of Alzheimer's disease, J. Alzheimers Dis. 35 (2013) 349–361.
[21] Y. Kia, H. Osman, R.S. Kumar, V. Murugaiyah, A. Basiri, S. Perumal, H.A. Wahab, C.S. Bing, Synthesis and discovery of novel piperidone-grafted mono- and bis-spirooxindole-hexahydropyrrolizines as potent cholinesterase inhibitors, Bioorg. Med. Chem. 21 (2013) 1696–1707.
[22] N.C. Inestrosa, A. Alvarez, C.A. Pérez, R.D. Moreno, M. Vicente, C. Linker, O.I. Casanueva, C. Soto, J. Garrido, Acetylcholinesterase accelerates assembly of amyloid-b-peptides into Alzheimer's fibrils: possible role of the peripheral site of the enzyme, Neuron 16 (1996) 881–891.
[23] L. Piazzi, A. Rampa, A. Bisi, S. Gobbi, F. Belluti, A. Cavalli, M. Bartolini, V. Andrisano, P. Valenti, M. Recanatini, 3-(4-{[Benzyl(methyl)amino]methyl} phenyl)-6,7-dimethoxy-2H-2-chromenone (AP2238) inhibits both acetylcholinesterase and acetylcholinesterase-induced β-Amyloid Aggregation: A dual function lead for Alzheimer's disease therapy, J. Med. Chem. 46 (2003) 2279–2282.
[24] A.S. Girgis, Regioselective synthesis of dispiro[1H-indene-2,3′-pyrrolidine-2′,3″-[3H]indole]-1,2″(1″H)-diones of potential anti-tumor properties, Eur. J. Med. Chem. 44 (2009) 91–100.
[25] B. Yu, D. Yu, H. Liu, Spirooxindoles: Promising scaffolds for anticancer agents, Eur. J. Med. Chem. 97 (2015) 673–698.
[26] R.F. George, N.S.M. Ismail, J. Stawinski, A.S. Girgis, Design, synthesis and QSAR studies of dispiroindole derivatives as new antiproliferative agents, Eur. J. Med. Chem. 68 (2013) 339–351.
[27] A.S. Girgis, S.S. Panda, A.M. Srour, H. Farag, N.S.M. Ismail, M. Elgendy, A.K. Abdel-Aziz, A.R. Katritzky, Rational design, synthesis and molecular modeling studies of novel anti-oncological alkaloids against melanoma, Org. Biomol. Chem. 13 (2015) 6619–6633.
[28] M.J. Kornet, A.P. Thio, Oxindole-3- spiropyrrolidines and piperidines. Synthesis and local anesthetic activity, J. Med. Chem. 19 (1976) 892–898.
[29] C. Marti, E.M. Carreira, Construction of spiro[pyrrolidine-3,3′-oxindoles] – recent applications to the synthesis of oxindole alkaloids, Eur. J. Org. Chem. (2003) 2209–2219.
[30] C.V. Galliford, K.A. Scheidt, Pyrrolidinyl-spirooxindole natural products as inspirations for the development of potential therapeutic agents, Angew. Chem. Int. Ed. 46 (2007) 8748–8758.
[31] B.M. Trost, M.K. Brennan, Asymmetric syntheses of oxindole and indole spirocyclic alkaloid natural products, Synthesis 18 (2009) 3003–3025.
[32] Y. Kia, H. Osman, R.S. Kumar, A. Basiri, V. Murugaiyah, Ionic liquid mediated synthesis of mono- and bis-spirooxindole-hexahydropyrrolidines as cholinesterase inhibitors and their molecular docking studies, Bioorg. Med. Chem. 22 (2014) 1318–1328.
[33] A.I. Almansour, R.S. Kumar, N. Arumugam, A. Basiri, Y. Kia, M.A. Ali, M. Farooq, V. Murugaiyah, A facile ionic liquid promoted synthesis, cholinesterase inhibitory activity and molecular modeling study of novel highly functionalized spiropyrrolidines, Molecules 20 (2015) 2296–2309.
[34] A. Basiri, B.M. Abd Razik, M.O. Ezzat, Y. Kia, R.S. Kumar, A.I. Almansour, N. Arumugam, V. Murugaiyah, Synthesis and cholinesterase inhibitory activity study of new piperidone grafted spiropyrrolidines, Bioorg. Chem. 75 (2017) 210–216.
[35] A.S. Girgis, Regioselective synthesis and stereochemical structure of anti-tumor active dispiro[3H-indole-3,2′-pyrrolidine-3′,3″-piperidine]-2(1H),4″-diones, Eur. J. Med. Chem. 44 (2009) 1257–1264.
[36] A.S. Girgis, J. Stawinski, N.S.M. Ismail, H. Farag, Synthesis and QSAR study of novel cytotoxic spiro[3H-indole-3,2′(1′H)-pyrrolo[3,4-c]pyrrole]-2,3′,5′(1H,2′aH,4′H)-triones, Eur. J. Med. Chem. 47 (2012) 312–322.
[37] University of Florida 2001–2005, CODESSA PRO. Available online: http://www.codessa-pro.com/index (accessed on Jun. 15, 2018).
[38] R.A. Copeland, Evaluation of Enzyme Inhibitors in Drug Discovery: A Guide for Medicinal Chemists and Pharmacologists, second ed., John Wiley & Sons, 2005.